Breast Cancer Research

RESEARCH

Open Access

Development of a humanized anti-FABP4 monoclonal antibody for potential treatment of breast cancer

Jiaqing Hao[1†], Rong Jin[2†], Yanmei Yi[3†], Xingshan Jiang[1], Jianyu Yu[1], Zhen Xu[4], Nicholas J. Schnicker[4], Michael S. Chimenti[5], Sonia L. Sugg[6] and Bing Li[1*]

Abstract

Background Breast cancer is the most common cancer in women diagnosed in the U.S. and worldwide. Obesity increases breast cancer risk without clear underlying molecular mechanisms. Our studies demonstrate that circulating adipose fatty acid binding protein (A-FABP, or FABP4) links obesity-induced dysregulated lipid metabolism and breast cancer risk, thus potentially offering a new target for breast cancer treatment.

Methods We immunized FABP4 knockout mice with recombinant human FABP4 and screened hybridoma clones with specific binding to FABP4. The potential effects of antibodies on breast cancer cells in vitro were evaluated using migration, invasion, and limiting dilution assays. Tumor progression in vivo was evaluated in various types of tumorigenesis models including C57BL/6 mice, Balb/c mice, and SCID mice. The phenotype and function of immune cells in tumor microenvironment were characterized with multi-color flow cytometry. Tumor stemness was detected by ALDH assays. To characterize antigen-antibody binding capacity, we determined the dissociation constant of selected anti-FABP4 antibodies via surface plasmon resonance. Further analyses in tumor tissue were performed using 10X Genomics Visium spatial single cell technology.

Results Herein, we report the generation of humanized monoclonal antibodies blocking FABP4 activity for breast cancer treatment in mouse models. One clone, named 12G2, which significantly reduced circulating levels of FABP4 and inhibited mammary tumor growth, was selected for further characterization. After confirming the therapeutic efficacy of the chimeric 12G2 monoclonal antibody consisting of mouse variable regions and human IgG1 constant regions, 16 humanized 12G2 monoclonal antibody variants were generated by grafting its complementary determining regions to selected human germline sequences. Humanized V9 monoclonal antibody showed consistent results in inhibiting mammary tumor growth and metastasis by affecting tumor cell mitochondrial metabolism.

Conclusions Our current evidence suggests that targeting FABP4 with humanized monoclonal antibodies may represent a novel strategy for the treatment of breast cancer and possibly other obesity- associated diseases.

Keywords FABP4, Monoclonal antibody, Breast cancer, ALDH

†Jiaqing Hao, Rong Jin and Yanmei Yi contribute equally to this work.

*Correspondence:
Bing Li
bing-li@uiowa.edu

Full list of author information is available at the end of the article

Background

Surpassing lung cancer for the first time in 2020, breast cancer has become the most common cancer in women diagnosed in the U.S. and worldwide [1]. The incidence of breast cancer has increased dramatically from 641,000 cases in 1980 to more than 2.3 million in 2020[1, 2]. Despite new treatment options in improving survival, around 685,000 women still die of breast cancer worldwide annually [1]. Multiple risk factors, including genetic mutations and background, family and reproductive history, aging and exposures to toxins, contribute to breast cancer risk. However, the global rates of breast cancer incidence and mortality have continuously increased in the past few decades [2], suggesting that other etiological factors besides the above-mentioned factors contribute to the increasing rates of breast cancer.

Obesity is a complex condition with multiple contributing factors, including genetics, environment, behavior, and metabolism [3, 4]. In modern society, owing to excessive calorie intake and a sedentary lifestyle [5, 6], obesity has risen at an alarming rate in the U.S. According to CDC statistics, adult obesity prevalence reached 42.4% in 2017–2018. Nearly half of Americans are projected to become obese by 2030. As a result, extra energy stored as lipids in various cells and tissues can negatively affect cell metabolism and homeostasis. In obese patients, adipose tissue contains crown-like structures formed by hypertrophic adipocytes surrounded by macrophages [7]. The interaction between macrophages and adipocytes promotes obesity-associated chronic inflammation and further pathological alterations. As an endocrine organ, adipose tissue produces multiple mediators (e.g., adipokines, cytokines, chemokines and hormones) to maintain metabolic balance. Dysregulation of these mediators is correlated with obesity-associated diseases, including at least 13 types of cancer [8]. Epidemiologic studies have confirmed that obesity increases not only the risk of breast cancer in postmenopausal women, but also the mortality from breast cancer in women of all ages [9–11].

Given the prevalence of obesity and increased risk of breast cancer in obese patients, several cellular and molecular mechanisms have been proposed to explain the obesity/cancer axis, which includes cancer-associated adipocytes, obesity-related inflammatory cytokines (e.g.,IL-6 and TNFα), lipids (e.g., lysophosphatidic acid and prostaglandins), adipokines (e.g., leptin and adiponectin), insulin/insulin-like growth factors (IGFs), and sex hormones [8, 12, 13]. Although substantiated by significant clinical and experimental data, these mechanisms remain contentious due to the complex multisystem interactions between obesity and cancer [14]. In exploring obesity/breast cancer risk, we have identified adipose fatty-acid binding protein (A-FABP, also known as FABP4, aP2) as a new molecular mechanism linking obesity-associated breast cancer development [15–17]. Traditionally recognized as an intracellular lipid chaperone, FABP4 is mainly expressed in adipose tissue, facilitating fatty-acid transportation, metabolism and responses [18, 19]. However, we demonstrate that obesity elevates FABP4 secretion from adipose tissue into the circulation, where extracellular FABP4 can directly target breast cancer cells, enhancing IL-6/STAT3/ALDH1-mediated tumor stemness and aggressiveness [15, 16]. Circulating FABP4 bridges tumor-associated stromal cells to tumor stem cells and integrates adipokines to tumor-promoting signaling and lipid metabolism, thereby representing a new molecular link underlying obesity-associated breast cancer risk and mortality. Therefore, targeting circulating FABP4 represents a novel strategy for treatment of breast cancer.

In the current study, we immunized mice with recombinant FABP4 protein and screened over 1200 hybridoma clones. We identified one clone, 12G2, which was able to effectively block FABP4 activity and inhibit mammary tumor growth in different mouse models. After evaluating the efficacy of its chimeric version and humanized variants, we successfully generated a humanized FABP4 monoclonal antibody (mAb), which offers potential for treating breast cancer in the clinic.

Materials and methods

Generation of mouse monoclonal antibody

FABP4 mAbs were generated by immunization of 7-week-old female FABP4 knockout mice with full length human recombinant FABP4 protein as previously described [20]. Briefly, 50 μg protein emulsified with complete Freund's adjuvant (Cat. #F5506-10ML from MilliporeSigma) was subcutaneously (s.c.) injected into the back of the mice. Mice were boosted with 25 μg protein mixed with incomplete Freund's adjuvant (IFA, Cat. #P9622-10×1ML from MilliporeSigma) by s.c. at day 14 and day 28. The final boosting was conducted at day 50 with 25 μg protein mixed with IFA by intravenous injection. Blood from immunized mice was collected for measurement of anti-FABP4 antibodies by ELISA. Mice with a high titer of anti-FABP4 antibodies were selected for splenocyte collection and fusion with Sp2/0 myeloma cells (ATCC). Hybridoma generation was performed using the ClonalCell^{TM}-HY kit (Cat. #03800 from STEMCELL Technologies). Of note, compared to conventional hybridoma selection and cloning, this method uses a methylcellulose-based semi-solid medium, which increases the diversity of clones that can be easily identified and isolated, enabling hybridoma selection and cloning to complete in a single step [21]. On day 12 after fusion, a total of 1248 single clones in the semi-solid medium were collected and cultured for another 4–7 days. The supernatants were screened for reactivity to

human recombinant FABP4 or FABP5 by ELISA. A total of 141 positive clones to FABP4 were selected for further screening with other sources of human or mouse FABP4 protein (Cat. #10,009,549 from Cayman Chemical). Finally, 25 positive clones with specific reactivity to both human and mouse FABP4, but not FABP5, were identified. These which were able to produce ample ascites and with better affinity to FABP4 were selected for antibody production.

Antibody purification from ascites

Ascites of the selected clones of hybridoma cells were developed in 8-week-old female Balb/c mice (n=6–7 mice/group). Briefly, 0.5 ml pristane was intraperitoneally (i.p.) injected into each mouse. After pristane priming for 7–10 days, 5×10^6 hybridoma cells in 400 µl PBS were i.p. injected into each mouse. Ascites developed 5–7 days after hybridoma cell injection were harvested from the second week using the 19-gauge needles. Cellular components in the ascites were removed by centrifugation at 2000 rpm for 15 min. The monoclonal antibody purification was performed as previously described [22, 23]. In our procedure, ascites was diluted by adding 4 volumes of 60mM acetate buffer with a final pH of 4.5. Caprylic acid (Cat. #C2875-10ML from MilliporeSigma) was added slowly to the ascites with continuous stirring to ensure thorough mixing. The final concentration of caprylic acid in the ascites was 25 µl/ml. The mixture was stirred for 30 min and then centrifuged for 30 min at 10,000 g. The supernatant was collected and mixed with 1/10 volume 10x PBS after nylon mesh filtration. After pH adjustment to 7.4, ammonium sulfate (0.277 g/ml) was slowly added to the solution at 4 °C and stirred for additional 30 min before centrifugation for 30 min at 5000 g. The precipitated antibody was resuspended in small volume of PBS. The purity and quantification of different monoclonal antibodies were determined by SDS-PAGE analysis and BCA quantification, respectively. Antibodies with purity > 85% were used for further applications.

Evaluation of antibody therapeutic efficacy using breast cancer mouse modes

Mouse models of breast cancer were used to evaluate the potential therapeutic efficacy of different clones of the purified FABP4 antibodies, as described above. Mouse experiments were performed according to the approved procedures by the Institutional Animal Care and Use Committee (IACUC) at the University of Iowa. To investigate the effect of antibody produced by hybridoma cells, 0.5 ml pristine was injected intraperitoneally into the Balb/c mice on day 0 to prime the antibody production. On day 7, 12G2 hybridoma cells (5×10^6 cells in 100 µl PBS /mouse) and control Sp2/0 cells (5×10^6 cells in 100 µl PBS/mouse) were injected intraperitoneally into separate groups of mice. MMT tumor cells (1×10^6 cells in 100 µl PBS/mouse) were orthotopically injected into the mammary fats pads to monitor tumor growth. To further test the efficacy of purified 12G2 antibody from ascites, C57BL/6-derived mammary tumor cells E0771 (5×10^5 cells in 100 µl PBS/mouse) and highly aggressive Balb/c-derived 4T1 tumor cells (1×10^5 cells in 100 µl PBS/mouse) were orthotopically injected into mammary fats of C57BL/6 mice or Balb/c mice (8–10 weeks old), respectively. After tumor injection, mice were randomly divided into several groups and treated with different clones of purified antibodies (5 mg-30 mg/kg, twice/week). Mice treated with the same volume of PBS were used as controls. When the tumors were palpable, the length and width of the tumors were measured by a caliper every three days. The volume of the tumors was calculated using the formula of 0.5 x length x width [24] as described before [25, 26]. To monitor antibody efficacy against human breast cancer, MCF7 cells were utilized in a xenograft mouse model. Matrigel (Cat. # 354,262 from Corning) was mixed with MCF7 cells in PBS (Matrigel/PBS=1:1) and injected (3×10^6 cells in 100 µl mixture/mouse) using a 23G needle into mammary fat pads of SCID mice. Tumor growth was monitored in antibody- or PBS-treated mice similarly to the method described above.

Production of chimeric and humanized anti-FABP4 antibodies

For chimeric antibodies, anti-FABP4 hybridoma clones (e.g., 12G2, 6H10) were sequenced and DNA sequences of the VH and VL regions were identified. Recombinant chimeric antibodies consisting of mouse VH and VL and human IgG1 constant regions were expressed and purified in HEK293 cells. For humanized antibody production, parental VH and VL sequences were run through a CDR grafting algorithm to transfer the CDRs from the original framework onto the most matched human germline sequences. To ensure that no highly undesirable sequence liabilities were introduced into the humanized sequences, identified high-risk motifs were removed through mutagenesis. A total of 16 antibody variants composed of different pairings of 4 humanized heavy chains and 4 humanized light chains were generated using HEK293 mammalian cells. All chimeric and humanized antibodies were made by Absolute Antibody (United Kington) with high purify and low endotoxin (<0.05EU/mg) for in vivo studies.

Aldehyde dehydrogenase (ALDH) assay

The ALDEFLUOR kit (Cat. #01700 from STEMCELL technologies) was used to detect ALDH activity for both tumor tissues and tumor cell lines. To obtain single cells from tumor tissues, E0771 and MCF7 tumors were

removed from euthanized mice and mechanically dissociated into smaller fragments. These fragments were then treated with 6 ml tri-enzyme solution containing 0.5 mg/ml collagenase type 2 (Cat. #LS004177 from Worthington Biochemical), 0.2 mg/ml hyaluronidase (Cat. #0215127590 from MP Biomedicals), and 0.02 mg/ml DNase I (Cat. #E1009-A from ZYMO research) in RPMI-1640 medium containing 5% FBS and incubated at 37 °C for 45 min on an orbital shaker at speed of 50 rpm. Following enzymatic digestion, the cell suspensions were collected by vortexing, filtration, removal of tri-enzyme solution, and two washes with cold 1x PBS. The detection of ALDH activity from both single- cell suspensions derived from tumor tissues and tumor cell lines were followed the protocol provided in the ALDEFLUOR kit.

Tumor migration, tumor invasion, and limiting dilution assays

To assess the blocking activity of anti-FABP4 antibodies, the molar ratio of antibody to FABP4 antigen was set at 1: 2. Individual antibodies (1 μg/ml) and human FABP4 protein (200ng/ml) were mixed for 15 min before performing following assay. FABP4 and PBS alone were served as controls. (1) wound-healing migration was performed to assess whether antibodies were able to inhibit FABP4-mediated tumor cell migration. To induce a linear wound in the cellular monolayer, the confluent cells were mechanically scratched using a 200 μL plastic pipette tip in a six well-plate containing 2.5 ml cell culture medium. Subsequently, the scratched monolayer was carefully washed with pre-warmed 1 x PBS to eliminate any debris. Following a 96-hour incubation period at 37 °C, the migration of cells towards the wound site was captured using light microscopy, and the migration area was quantified using Image J software. (2) For tumor invasion assay, MCF-7 cells were cultured to form spheres in hanging drops of culture medium on the lid of cell culture dishes as previously described [16]. Briefly, following a seven-day incubation period, the spheroids from the lid were transferred into an equivalent volume and combined with rat tail type I collagen (Cat. #A1048301 from Fisher Scientific), reaching a final concentration of 1.7 mg/ml. This mixture was then embedded in a 24-well plate to establish a 3D culture system. FABP4/antibody mixture, FABP4 protein and control PBS were added into 1 ml cell culture medium, respectively. Quantitative analyses were performed by measuring the maximal invasive distance (longest distance from the spheroid radius) and the invaded area (total invaded area minus the spheroid area) using Image J software. (3) For in vitro limiting dilution assay (LDA), tumor cells were serially diluted to obtain cell concentration at a range of 1000, 500, 250, 125, 62, 31, 16, 8 cells and seeded into an ultra-low attachment 96-well plate containing 200 μL cell culture medium, exposed to FABP4-antibody mixture, FABP4 protein and control PBS for a duration of 48–96 h. Subsequently, cell spheres were determined using microscope and calculated the cancer cells initiating frequency and significance using online software (Extreme limiting dilution analysis, ELDA @ http://bioinf.wehi.edu.au/software/elda/index.html) following the methodology outlined by Hu and Smyth [27].

Characterization of antibody/antigen binding

The binding of anti-FABP4 antibodies with FABP4 was evaluated by ELISA and BIAcore assays. For ELISA, FABP4 protein or biotinylated FABP4 epitope peptides (Mimotopes) was diluted with 1 x PBS and coated either to a non-coated 96-well plate or to a streptavidin-coated 96-well plate at a final volume of 100 μL overnight. After blocking with 5% BSA at room temperature for 1 h, anti-FABP4 antibodies (e.g., chimeric, humanized) were diluted with 5% BSA solution and added into indicated wells. The plate was washed three times using 200 μL of 1 x PBS containing 0.5% Tween-20 and incubated with 100 μL of secondary antibody solution containing goat anti-human IgG conjugated with HRP (Cat. #A18805 from Invitrogen) at a dilution of 1:10000 in 5% BSA solution for 1 h. Color development was performed by adding 100 μL of substrate solution and incubating for 5 min at room temperature before the reaction was stopped by 100 μL of 2 N sulfuric acid. OD value was acquired using a BioTek Synergy LX Multimode Reader. Binding affinity measurement was performed by ProteoGenix (France). Briefly, human FABP4 (10 μg/ml) was immobilized on CM5 sensor chip of BIAcore 8 K using maleimide EDC/NHS coupling. A stable cell pool of 12G2 V9 antibody (s-V9) was produced using Chinese hamster ovary (CHO) cells (ProteoGenix, France). Antibody (s-V9) at a defined concentration (ranging from 0.156 to 2.5μM) was flowed over CM5 chip and response captured over time, showing the progress of the interaction and association/dissociation cycle. After different concentrations are successively tested, the kinetics parameters and affinity are calculated using the BIA-evaluation software.

Immunophenotype analysis by flow cytometry

Immune phenotypes were performed using multi-color staining panel designed by improved version of full spectrum viewer in Cytek Cloud. Signle-cell suspension of the primary tumor was resuspended in 1 x PBS containing 0.5% FBS and kept in the ice all the time. Cells were pre-incubated with anti-mouse CD16/CD32 antibody (Cat. # 101,302 from Biolegend) for 5 min to block Fc receptors. Surface staining was prepared using the following antibodies: Zombie-violet (Cat. #423,108, Biolegend), anti-mouse CD45 (Cat. #103,116, Biolegend), anti-mouse CD11b (Cat. #612,800, BD), anti-mouse

CD3 (Cat. #100,355, Biolegend), anti-mouse CD4 (Cat. #740,208, BD), anti-mouse CD8 (Cat. #752,642, BD), anti-mouse F4/80 (Cat. #123,120, Biolegend), anti-mouse MHCII (Cat. #107,604, Biolegend), anti-mouse Ly6G (Cat. #127,664, Biolegend), anti-mouse NK1.1 (Cat. #108,736, Biolegend), anti-mouse B220 (Cat. #103,232, Biolegend), and anti-mouse CD11c (Cat. #117,349, Biolegend). The intracellular cytokines staining with anti-mouse IL-6 (Cat. #504,508, Biolegend) and anti-mouse TNFα (Cat. #506,338, Biolegend) were fixed and permeabilized using True-Nuclear transcription factor buffer set (Cat. #424,401 from Biolegend) according to the manufacturer's introduction. All samples were acquired with an Cytek Aurora instrument. Data were analyzed with FlowJo (BD).

Spatial transcriptomics and analysis

Fresh tumor tissues were removed and placed in a petri-dish and embedded with room temperature OCT without any bubbles on the tissue's surface. The embedded samples were transferred into the cryo mold. The cryo mold containing OCT-embedded samples were put into the metal beaker with 2-methylbutane in a dewar of liquid nitrogen until the OCT was solidified. Sample cryosectioning, affixment to cDNA capture slide, H&E staining, tissue permeabilization, RNA capture, and cDNA synthesis were performed according to the 10 x Genomics Visium spatial transcriptomics' methods.

The four visium libraries (two PBS tumors, and two S-V9-treated tumors) were sequenced on an Illumina NovaSeq 6000 located in the Iowa Institute of Human Genetics (IIHG) Genomics division. Paired-end reads were demultiplexed and converted from the native Illumina BCL format to fastq format using an in-house python wrapper to Illumina's 'bcl2fastq' conversion utility. The data were deposited to GEO repository (GSE264099). Bioinformatic analysis was carried out by the IIHG Bioinformatics division. Fastq data were merged across lanes and the PE reads were used as input for the 10X SpaceRanger pipeline in 'count' mode (v1.3.1). SpaceRanger was run on the Argon High-Performance Computing (HPC) cluster at the University of Iowa using 32 cores and 128GB of RAM per sample. The reference transcriptome was specified as 'mm10-2020-A' and the chemistry was specified as 'Spatial 3' v1'. QC analysis of the four samples showed no quality problems for each sample other than an alert that "Low Fraction Reads in Spots" was detected for 3 of 4 samples. Filtered barcode matrices were used as input for downstream analysis in Seurat (v5). Four Seurat objects were created from the individual barcode matrices and quality control (QC) metrics were visualized as violin plots that included the number of genes (nFeature), number of UMI (nCount) and percentage of mitochondrial UMI (percent_mt). We filtered cells that have less than 100 features (low-quality cells). The filtered datasets were subjected to normalization, detection of variable features, scaling/centering and PCA analysis. Following this, the sample layers were integrated together using the "RPCA" method of integration available in Seurat 5 (https://satijalab.org/seurat/articles/integration_rpca). To cluster the cells, we used K-nearest neighbors (KNN) networks based on the calculated PCs. Modularity optimization was applied (Louvain method, resolution = 0.1) and a UMAP embedding was calculated. Searching for DEGs (cluster biomarkers), we found markers for every cluster compared with all remaining cells using the Wilcoxon Rank Sum test and a $\log_2$FC threshold of 0.4 and expressed in more than 30% of the cells. Cluster-wise DE analysis of the treatment effect of S-V9 vs PBS was carried out by using the "FindMarkers" function on the integrated object. Pathway analysis was carried out using g: Profiler (https://biit.cs.ut.ee/gprofiler/gost) and iPathwayGuide software (AdvaitaBio).

H&E staining

Fresh tissues were obtained after removing primary tumor from euthanized mice. Lung samples were collected from the right inferior lobe and fixed immediately in 10% neutral buffered formalin. Air microbubbles were removed by placing lungs in a vacuum chamber for 5 min, then re-fixed the lungs into the fresh 10% neutral buffered formalin for 24 h. Following serial alcohol dehydration (50%, 75%, 95%, and 100%), the samples were embedded in paraffin. The paraffin-embedded samples were sliced into 8 µm sections and stained in the DRS-601 Auto Stainer with hematoxylin and eosin (H&E) for 1 min. Slides were mounted with VectaMount® Express Mounting Medium (vector laboratories, H-5700-60), and were scanned by slide scanner (Leica Aperio GT 450) for quantification analysis. The metastatic tumor number and area was analyzed by the SlideViewer 2.7.0.191696 software.

Quantification of serum biomarkers

Serum samples were collected at the end point of tumor challenge mouse model. Samples from each mouse were divided into aliquots and preserved in an -80 C freezer for future purposes. The quantification of FABP4 (Cat. #CY-8077, MBL), IL-6 (Cat. #431,301, Biolegend) and glucose (Cat. #81,692, Crystal Chem) levels were performed separately using ELISA kits in accordance with the instructions provided by the manufacturers.

Statistical analysis

All data were presented as the mean ± SD unless notified specifically. For in vitro and in vivo experiments involving two groups, a two-tailed, unpaired Student's t-test was performed by GraphPad Prism 9. For experiments

containing more than two groups, a two-way ANOVA with multiple comparison test was used by GraphPad Prism 9. Statistical significance was defined as a p-value of less than 0.05.

Results

Generation of anti-FABP4 monoclonal antibodies in mice

Human and mouse FABP4 share 92% amino acid sequence homology. To broaden the anti-FABP4 antibody epitope repertoire, we utilized FABP4 knockout mice and immunized them with recombinant human FABP4. Mice with high anti-FABP4 antibody titers were selected for hybridoma generation and clone selection (Figure S1A-S1C). After screening around 1248 clones in vitro, we identified at least 25 clones that were specifically bound to FABP4 but not to FABP5 (Table S1). Of these 25 clones, 6 clones were capable of inducing high-yield production of ascites (Table S1).

To evaluate the potential neutralizing effect of these clones, we measured serum FABP4 levels in mice before and after ascites production. One clone, named 12G2, correlated with significantly reduced serum levels of FABP4 (Fig. 1A). Interestingly, when MMT mammary tumor cells were implanted in mice with or without 12G2 ascites (Fig. 1B), MMT tumor growth and weight in mice with 12G2 ascites were significantly reduced compared to mice without 12G2 ascites (Fig. 1C and D). To verify the tumor inhibition effect, we purified antibodies from the 12G2 and two other clones (12H2 and 6H10) and used them to treat E0771, a commonly used breast cancer mouse model (Fig. 1E). Compared to the 12H2 (Figure S1D) and 6H10 (Figure S1E) clones, the 12G2 clone significantly inhibited E0771 tumor growth (Fig. 1F) and weight (Fig. 1G). Moreover, serum levels of FABP4 (Fig. 1H), IL-6 (Fig. 1I), but not glucose (Fig. 1J), were significantly reduced in response to 12G2 treatment. Altogether, these data suggest the 12G2 clone as a potential therapeutic monoclonal antibody targeting FABP4.

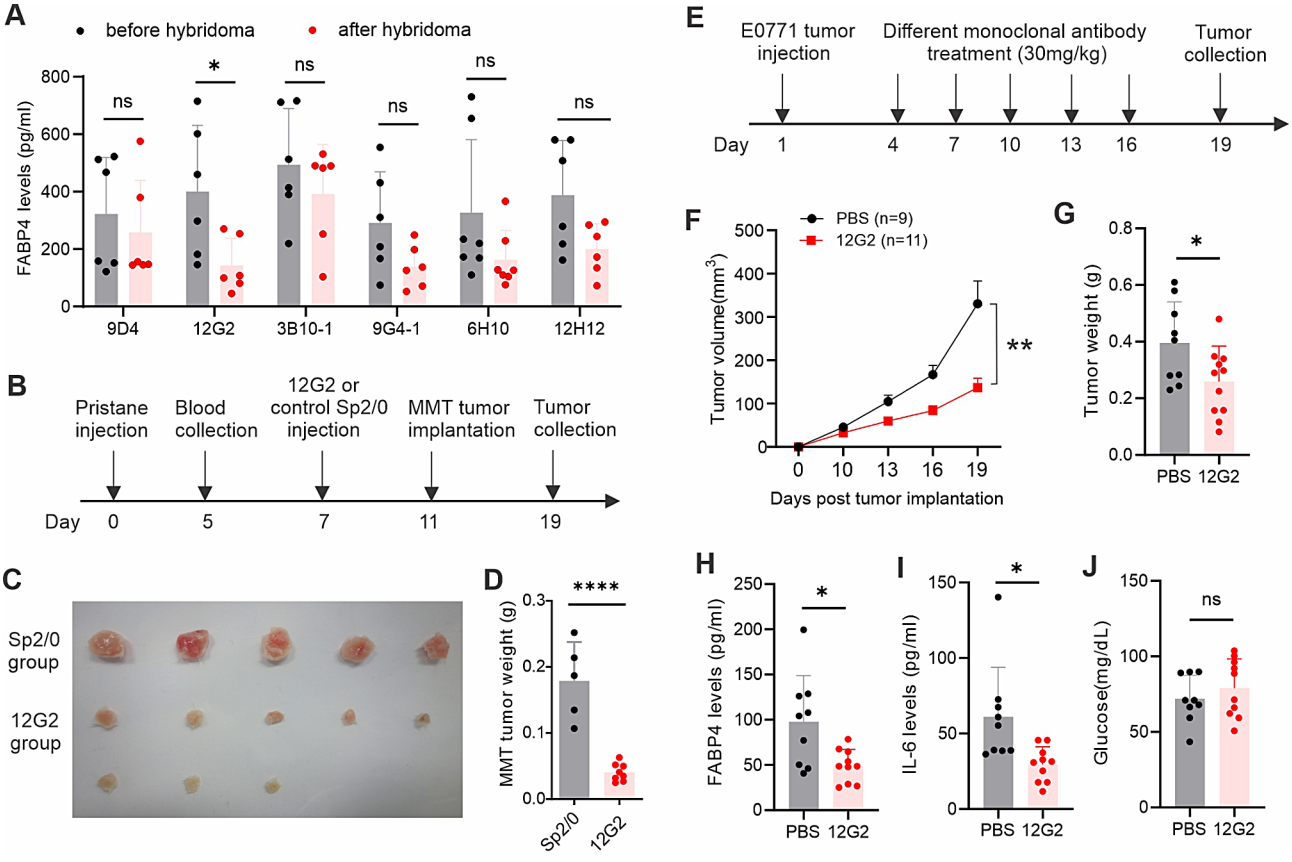

Fig. 1 Screening of anti-FABP4 mAbs for treatment of mammary tumors. Measurement of circulating FABP4 levels in mice before and after injection of different anti-FABP4 hybridoma clones by ELISA (*$p < 0.05$, ns, non-significant). (**A**) Schematic of evaluating the effect of anti-FABP4 hybridomas on MMT mammary tumor growth in vivo, **(C, D)** Tumor size **(C)** and weight **(D)** in mice injected with SP2/0 or 12G2 hybridoma, respectively (****$p < 0.0001$), **(E)** Schematic of evaluating the effect of purified 12G2 antibody on E0771 mammary tumor growth in vivo, **(F, G)** E0771 tumor growth curve **(F)** and weight **(G)** in mice treated with 12G2 antibody or PBS control, respectively (*$p < 0.05$, **$p < 0.01$), **(H-J)** Serum levels of FABP4 **(H)**, IL-6 **(I)** and glucose **(J)** in E0771 tumor-bearing mice treated with PBS or 12G2 antibody for 19 days (*$p < 0.05$, ns, non-significant)

Evaluation of the efficacy of chimeric mouse/human anti-FABP4 antibodies

To verify the therapeutic potential of the 12G2 clone, we generated chimeric mouse-human antibodies by joining the variable regions of 12G2 or 6H10 (as a control) to human IgG1 constant regions (Fig. 2A). After the purification of the two chimeric antibodies (Figure S2A), we used an MCF-7 xenograft model to test their therapeutic efficacy in vivo (Fig. 2B). Consistent with their parental clones, the chimeric 12G2 mAb exhibited better efficacy than 6H10 mAb in inhibiting MCF-7 tumor growth and size in SCID mice (Fig. 2C and D). Treatment with the chimeric 12G2 antibody also significantly reduced MCF-7 tumor weight in SCID mice (Fig. 2E). Interestingly, FABP4-mediated MCF-7 cell invasion and ALDH1 activity were significantly inhibited by the treatment of the chimeric 12G2 antibody (Fig. 2F and G, Figure S2B-S2D), further corroborating a specific role of 12G2 in blocking FABP4 activity in vitro. Moreover, using colony formation assays, we demonstrated that 12G2 significantly inhibited FABP4-induced colony-initiating cell frequency in different breast cancer tumor cell lines, including E0771, M158 and MCF7 (Figure S2E-S2G). Altogether, these in vitro and in vivo studies strongly supported the therapeutic efficacy of the chimeric 12G2 antibody.

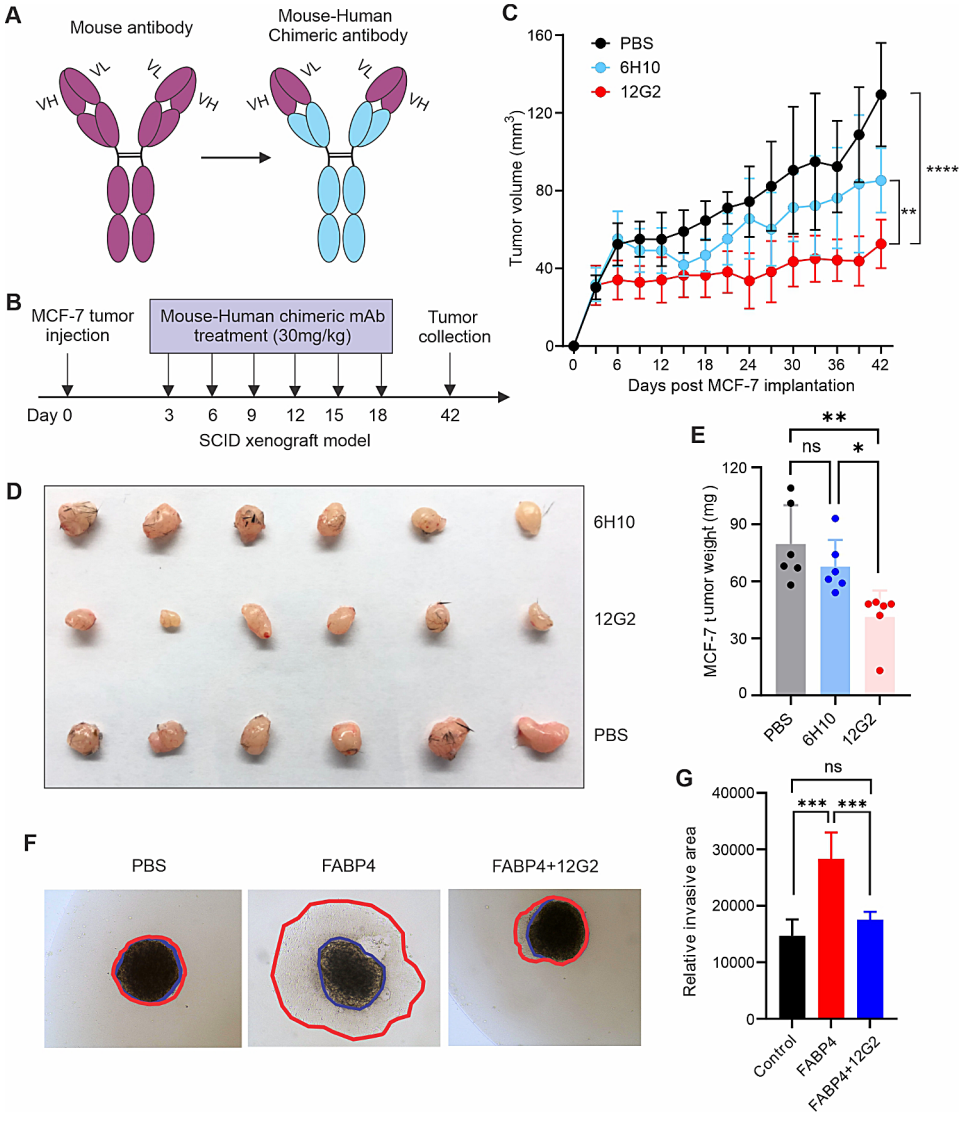

Fig. 2 Evaluating therapeutic and blocking activity of chimeric anti-FABP4 antibodies. (**A**) Schematic of production of chimeric anti-FABP4 antibodies. (**B**) Schematic of evaluating the efficacy of chimeric antibody using MCF-7 breast cancer model in vivo. (**C**) Tumor growth curve of MCF-7 tumor in SCID mice treated with chimeric 6H10, 12G2 or PBS, respectively (**, $p < 0.01$, ****$p < 0.0001$). (**D**) Tumor size of MCF-7 in mice treated with 6H10, 12G2 or PBS, respectively, for 6 weeks. (**E**) Tumor weight of MCF-7 in mice treated with 6H10, 12G2 or PBS, respectively, for 6 weeks (*, $p < 0.05$, **$p < 0.01$, ns: non-significant). **(F, G)**, Measurement of MCF-7 tumor cell invasion in the presence of PBS, FABP4 (100ng/ml), or FABP4 + 12G2 in vitro **(F)**. Tumor invasion areas in each group are shown in panel G (***$p < 0.001$, ns: non-significant)

Development of humanized 12G2 antibodies

To further humanize the 12G2 antibody, we first aligned the VH and VL sequences of 12G2 mAb with human germline sequences and selected the closest matched germline sequences. The complementary determining regions (CDRs) of 12G2 mAb were then grafted onto the selected human germline sequences with point mutations around the framework amino acids to create 16 humanized 12G2 antibody variants (Fig. 3A). We purified the 16 recombinant antibody variants (Figure S3A) and measured their binding affinity to FABP4. Variant 9, 10, 14, 15 showed the highest binding affinity to FABP4 (Fig. 3B). Using in vitro tumor wound healing assays, we demonstrated that FABP4-enhanced tumor migration could be blocked by these variants, especially by V9 (Figure S3B, S3C). Using in vivo MCF-7 tumor models (Fig. 3C), we further demonstrated that compared to other variants, the V9 antibody showed the best therapeutic efficacy in inhibiting MCF7 tumor growth (Fig. 3D), tumor weight (Fig. 3E) and tumor proliferation

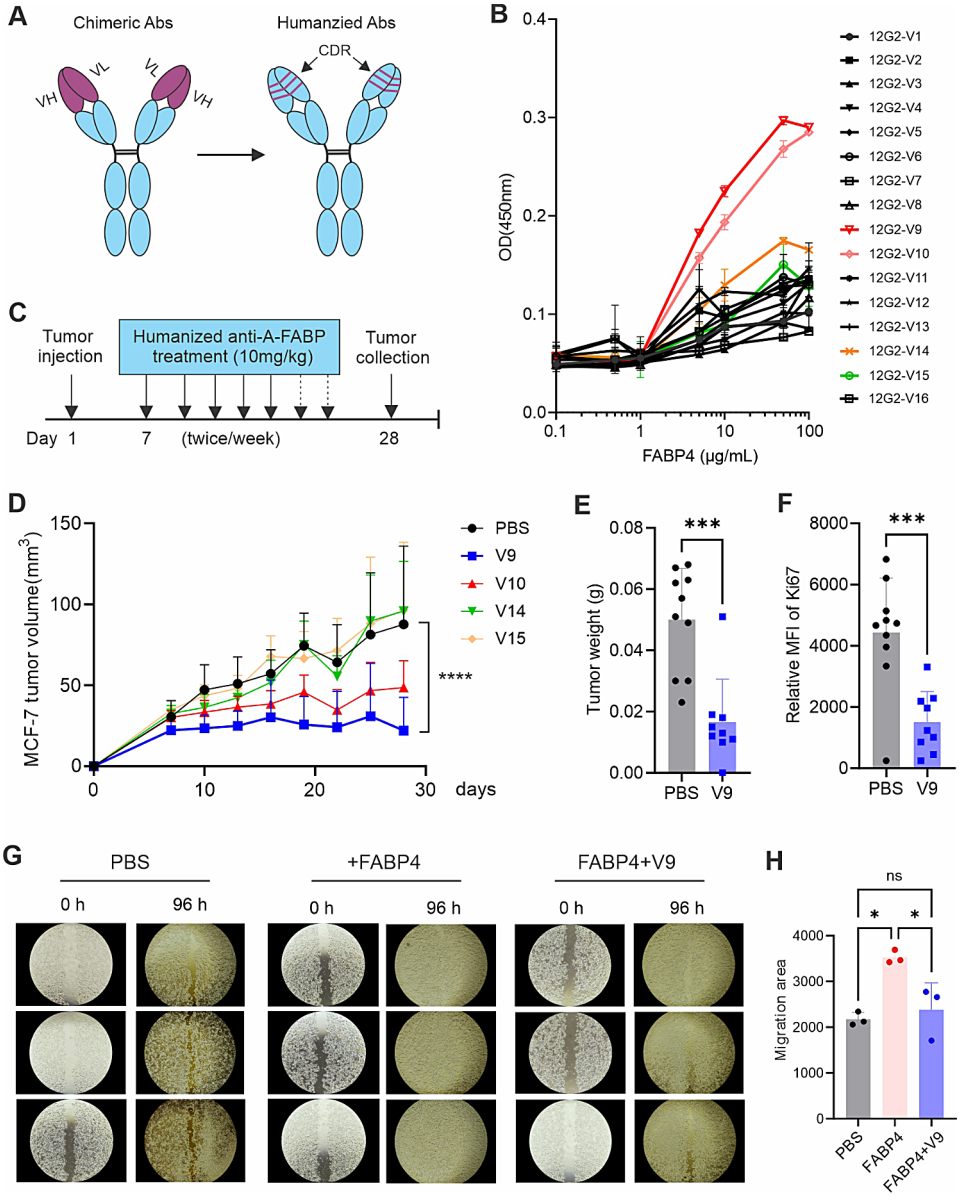

Fig. 3 (**A**) Assessing therapeutic and blocking activity of humanized 12G2 variants Schematic of production of humanized 12G2 antibody variants. (**B**) Measurement of 16 humanized 12G2 variants with FABP4 by ELISA. (**C**) Schematic of evaluating the efficacy of selected humanized 12G2 variants using MCF-7 breast cancer model in vivo. (**D**) Tumor growth curve of MCF-7 in SCID mice treated with V9, V10, V14, V15, or PBS, respectively (****$p < 0.0001$). (**E**) Comparison of tumor weight of MCF-7 in SCID mice treated PBS or V9 for 4 weeks (***$p < 0.001$). (**F**) Analysis of proliferation of MCF-7 cells by Ki67 expression in SCID mice treated with PBS or V9, respectively (***$p < 0.001$). **(G, H)** In vitro analysis of MCF-7 cell migration in the presence of PBS, FABP4 (100ng/ml) or FABP4 + V9, for 96 h. Migration area in each group is shown in panel H (* $p < 0.05$, ns, non-significant)

(Fig. 3F). Consistently, soluble FABP4 enhanced MCF-7 tumor cell migration compared to the PBS control. However, treatment with the V9 antibody successfully blocked the FABP4-mediated effect (Fig. 3G and H), supporting a specific role of this variant.

Confirming the therapeutic efficacy of V9 antibody using different mouse models

Our previous studies demonstrated that the deficiency of FABP4 inhibited E0771 tumor growth in syngeneic mouse models [17]. To compare the efficacy of the V9 antibody, we compared E0771 tumor growth in WT mice treated with or without V9 and in FABP4$^{-/-}$ mice. Tumor growth in mice treated with V9 antibody was significantly slowed down compared to those treated with the PBS control. Interestingly, the tumor growth rate in V9-treated mice was similar to that in FABP4$^{-/-}$ mice (Fig. 4A), suggesting that V9 antibody treatment exhibits an equal effect to FABP4 knockout. Moreover, E0771 tumor size and weight in V9-treated mice were similar to those in FABP4$^{-/-}$ mice (Fig. 4B and C). Consistent with our previous observations in FABP4$^{-/-}$ mice, V9 treatment reduced tumor stemness, as evidenced by reduced ALDH1 activity (Fig. 4D). V9 treatment also reduced the production of IL-6 but not TNFα in tumor-associated macrophages compared to PBS-treated mice (Figure S4A-S4D).

Obese mice exhibited elevated levels of circulating FABP4[17]. To test the efficacy of V9 antibody in obese mice, we fed SCID mice on a high fat diet for 15 weeks, and randomly grouped and treated them with V9 antibody or PBS control after the implantation of MCF-7

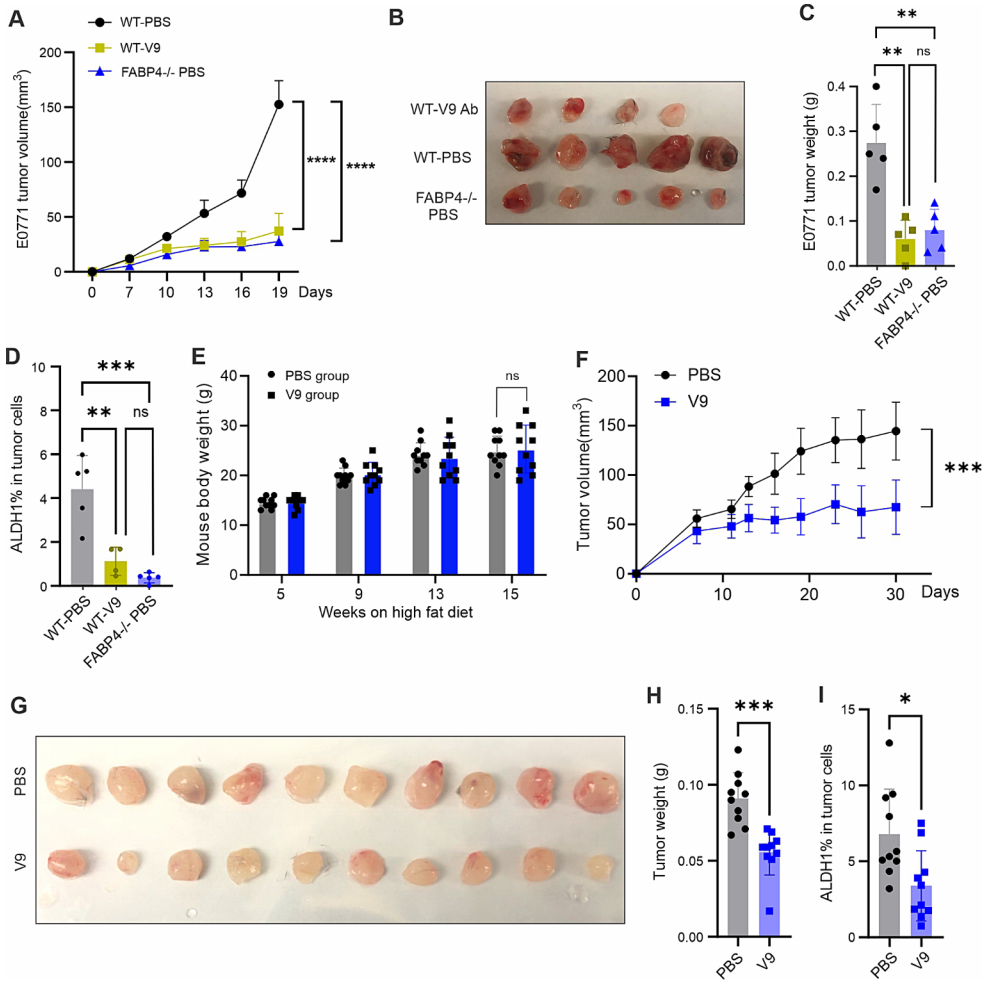

Fig. 4 Validation of the efficacy of humanized V9 antibody using different mouse models. (**A**) E0771 tumor growth curve in WT mice treated with PBS or V9 mAb (10 mg/kg) respectively. Tumor growth in FABP4$^{-/-}$ mice treated with PBS was used as a control (****$p < 0.0001$). (**B**) E0771 tumor size in WT mice treated with PBS or V9 mAb and in FABP4-/- mice treated with PBS. (**C**) E0771 tumor weight in WT treated with PBS or V9 mAb or in FABP4$^{-/-}$ mice treated with PBS (**$p < 0.01$, ns: non-significant). (**D**) Analysis of ALDH1 activity in E0771 tumors in mice treated with PBS or V9 mAb (**$p < 0.01$, ***$p < 0.001$, ns: non-significant). (**E**) Body weight of SCID mice fed with a HFD for 15 weeks (ns, non-significant). (**F**) MCF-7 tumor growth curve in HFD-fed SCID mice treated either with V9 mAb (10 mg/kg) or PBS control (****$p < 0.0001$), **(G, H)** MCF-7 tumor size **(G)** and weight **(H)** in HFD-fed SCID mice treated with V9 mAb or PBS, respectively (***$p < 0.001$), **(I)** Analysis of ALDH1 activity for MCF-7 tumors in HFD-fed SCID mice treated with PBS or V9 antibody ($p < 0.05$)

tumors in these mice (Fig. 4E). Consistently, the efficacy of V9 antibody treatment in obese mice was evident in the reduced rate of tumor growth (Fig. 4F), tumor size (Fig. 4G), tumor weight (Fig. 4H) and reduced ALDH1 activity in tumor cells (Fig. 4I). Notably, when we treated Balb/c mice implanted with highly aggressive 4T1 mammary tumor cells with the V9 antibody, we did not observe significant tumor growth inhibition (Figure S4E, S4F), suggesting that the efficacy of V9 was not universal for all types of breast cancer.

Characterization of the V9 antibody

To facilitate the translational potential of V9 antibody, we generated a stable cell pool of V9 antibody (S-V9) using CHO cells and characterized its binding properties of S-V9 antibody. First, we determined the dissociation constant (K_D) of S-V9 against FABP4 via surface plasmon resonance (BIAcore). Kinetic analysis of S-V9/FABP4 interaction showed that S-V9 had an overall K_D of 2.07×10^{-7}M with FABP4 (Fig. 5A). To delineate the precise binding epitopes of S-V9 on FABP4, we synthesized 25 peptides, each consistent of 15 amino acids (AA) with an overlap of 10 AA to cover the whole 132 AA sequence of FABP4 (Fig. 5B). These peptides were biotinylated at the N-terminus to enable binding measurement (Table S2). We demonstrated that peptides 1, 9, 11, and 18 exhibited strong binding to S-V9 (Fig. 5C), mapping the interaction epitopes to the β-1, β-2/3, β-3/4, and β-7 stand of the FABP4 structure (Fig. 5D, Figure S5A), respectively. The patten of epitope recognition by S-V9 distinguished it from other previous FABP4-targeting antibodies, CA33 and HA3 (Figure S5B), underscoring its potential for unique blocking mechanisms in therapeutic applications.

S-V9 mAb inhibits tumor growth and metastasis by disrupting mitochondrial energy metabolism

Using E0771 tumor models, we confirmed the efficacy of the S-V9 mAb in significantly inhibiting E0771 tumor growth, reducing tumor weight and decreasing tumor ALDH1 activity, as consistently observed (Fig. 6A C). The long-term therapeutic potential of S-V9 was further evaluated by treatment of E0771 tumor-bearing mice over a period exceeding six weeks. Notably, S-V9 treatment resulted in a robust inhibition of tumor growth (Figure S6A-S6B). In PBS-treated group, all mice developed lung metastasis, while half of S-V9 treated mice did not exhibit any lung metastasis (Figure S6C). The metastasis tumor nodules and nodular areas were significantly smaller in S-V9-treated mice compared to those in PBS-treated mice (Fig. 6D and E). Using Visium spatial single cell transcriptomic analysis (10X Genomics), we found that E0771 tumors exhibited 4 clusters using unsupervised KNN clustering at a resolution of 0.1 (Figure S6D). Remarkably, cells in cluster "1" were greatly reduced in response to antibody treatment while the proportion of cells in cluster "0" increased after treatment (Fig. 6F, Figure S6E). Among the top 10 marker genes in cluster "0", we found multiple immune cell markers, including IL1b, CCL4, S100a8, suggesting an overall immune cell population for the cluster "0". In cluster 1, breast cancer cell markers, including Nob1, Vmp1, Crk, Ckap2, Parp14 and Mfn1, were detected among the top cluster markers (Table S3). Expression of these cancer marker genes in cluster "1" were significantly reduced owing to antibody treatment (Fig. 6G and L), suggesting that S-V9 antibody treatment reduced cancer cell aggressiveness. Further analysis of differential expressed genes (DEG) in cluster "1" indicated that antibody treatment mainly affected pathways related to oxidative phosphorylation, mitochondrial protein-containing complexes, electron transport chain and ATP synthesis (Figure S6F). gProfiler human disease phenotypic analysis showed that S-V9 antibody treatment induced abnormal activity of mitochondrial respiratory chain and metabolism (Figure S6G). iPathwayGuide (AdvaitaBio) disease analysis also showed the top two hits to cluster "1" DEGs in response to antibody treatment were "Mitochondrial complex 1 deficiency" and "Combined oxidative phosphorylation deficiency", further confirming the previous analysis (Table S4). In contrast, the top hit to immune-related cluster "0" DEGs was inflammatory autoimmune disease "multiple sclerosis" (Table S5). Collectively, these results suggested that blocking FABP4 activity with the S-V9 antibody exerts a profound effect on mitochondrial energy metabolism of tumor cells, potentially contributing to the observed therapeutic outcomes.

Discussion

Based on the expression pattern of hormone receptors (HR) and human epidermal growth factor receptor 2 (HER2) on cancer cells, breast cancer generally falls into four subtypes as luminal A, luminal B, $HER2^+$ and triple-negative [28, 29]. As such, hormone or HER2-targeted therapies (such as Herceptin, anti-HER2 antibody) are used to treat luminal or $HER2^+$ patients. Due to the lack of receptors, triple-negative breast cancer represents the most difficult subtype to treat [30]. Given emerging roles of dysregulated lipid metabolism in cancer growth and metastasis [31, 32], blocking FABP4 activity represents a novel strategy for breast cancer treatment as it blocks lipid transportation and metabolism, thus inhibiting cancer cell growth and metastasis.

Bristol Myers-Squibb has developed a small molecular inhibitor, BMS309403, that binds FABP4 and inhibit its function [33]. Interestingly, mice treated with BMS309403 exhibited reduced symptoms of diabetes, atherosclerosis and mammary tumor growth [16, 34],

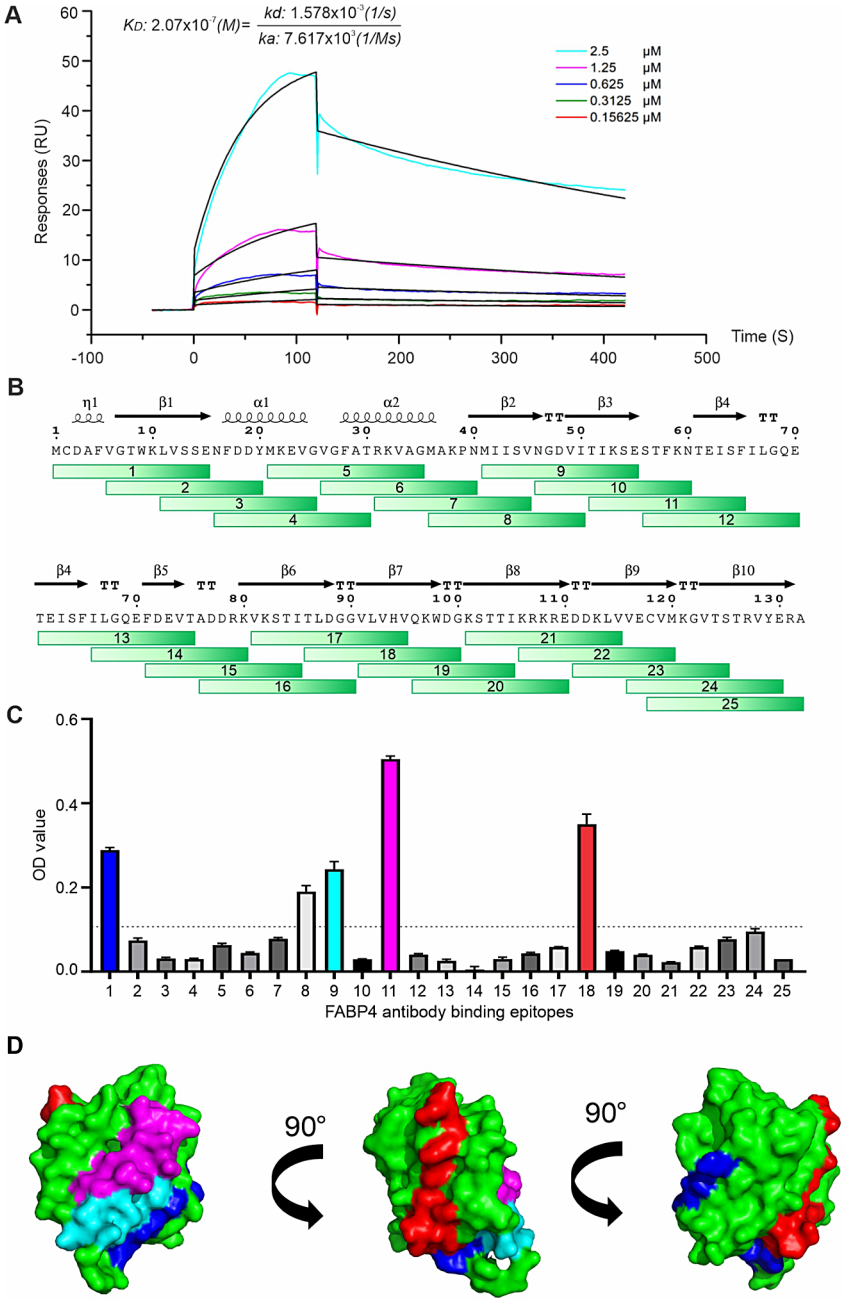

Fig. 5 Measurement of V9/FABP4 binding properties. (**A**) Analysis of K_D of V9/FABP4 interaction via SPR technology (BIAcore 8 K). (**B**) Synthesis of 25 overlapping peptides spanning the entire length of the FABP4 protein for epitope identification. (**C**) Measurement of V9 mAb binding peptides in FABP4 by ELISA. (**D**) Different angels of space-filling representation of FABP4/V9 mAb binding generated using the SWISS-MODEL

suggesting that targeting FABP4 with small-molecular inhibitors might represent a promising approach for treating obesity-associated diseases. However, like many other small-molecule drug candidates, in vivo applications of the BMS309403 demonstrated off-target activities [35, 36], and severe side-effects, including suppressing cardiac contractile function [37]. To eliminate the potential concerns related to small-molecule inhibitors, highly specific anti-FABP4 antibodies were developed to block the activity of circulating FABP4 in obese models [38, 39]. A rabbit polyclonal anti-FABP4 antibody was shown to reduce circulating FABP4 and to improve glucose tolerance in high fat diet-induced obese mice [38]. Subsequently, a rabbit-derived monoclonal anti-FABP4 antibody was developed with a therapeutic effect for treating type 2 diabetes in obese mice [39]. Notably, lean mice or humans exhibited relatively low levels of circulating FABP4, but tumor-bearing mice or

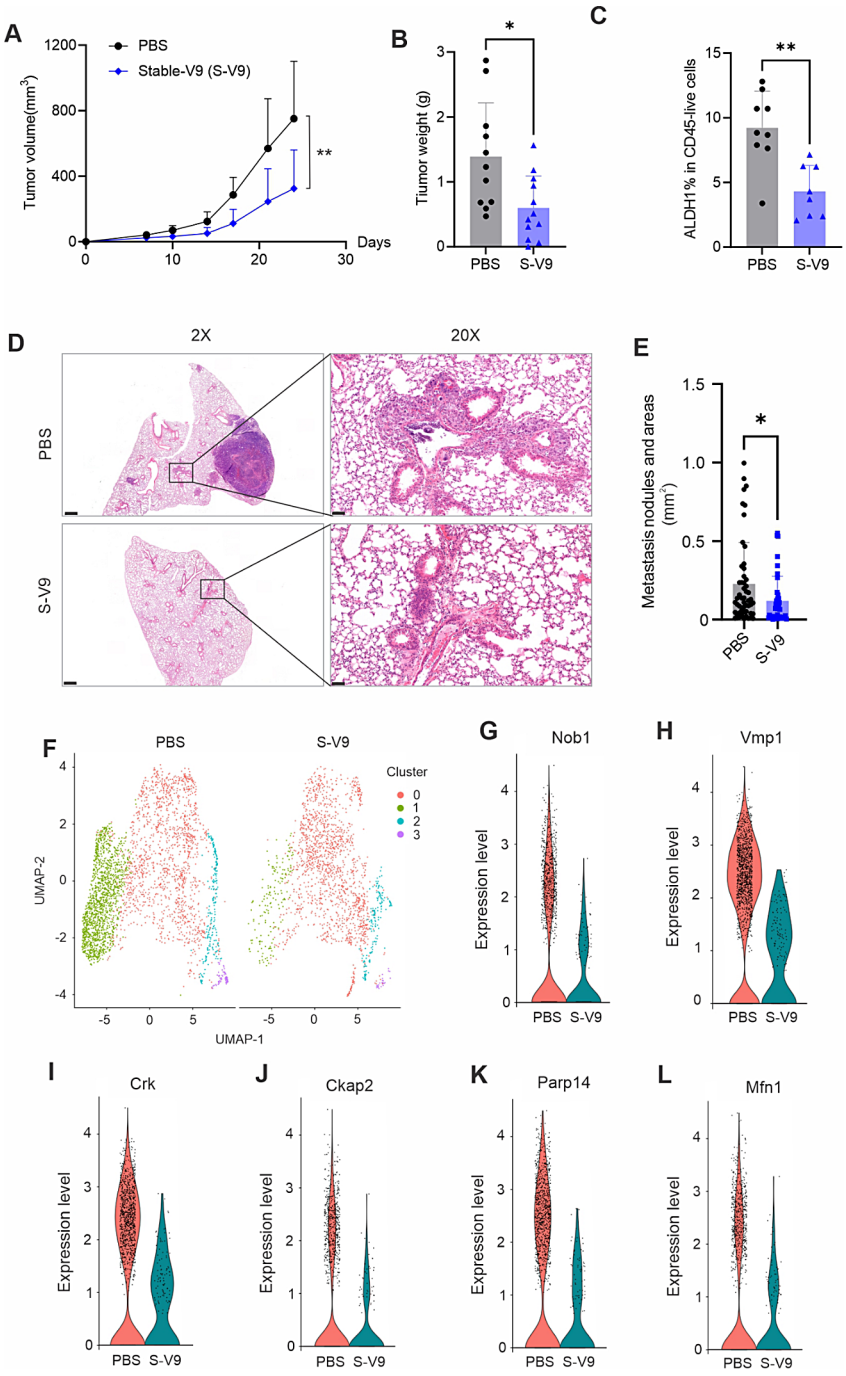

Fig. 6 S-V9 antibody treatment inhibits tumor growth and metastasis through inducing abnormal mitochondrial metabolism in tumor cells. (**A**) E0771 tumor growth curve in mice treated with PBS or S-V9 mAb (5 mg/kg) or PBS for 24 days (**$p < 0.01$). (**B**) E0771 tumor weight on 24 days post tumor implantation in mice treated with S-V9 mAb or PBS (*$p < 0.05$). (**C**) Analysis of ALDH1 activity in E0771 tumors in mice treated with S-V9 mAb or PBS, respectively (**$p < 0.01$), **(D, E)** Analysis of lung metastasis of E0771 tumor cells in mice treated with PBS or S-V9 mAb for 24 days by H&E staining (scale bar: 0.5 mm in 2X panel, 0.05 mm in 20x panel). Metastatic nodule numbers and areas are shown in panel E (*$p < 0.05$), **(F)** UMAP of unsupervised clusters in tumors treated with PBS or S-V9 mAb by spatial transcriptome analysis, **(G-L)** Violin plot of breast cancer cell markers, including Nob1 **(G)**, Vmp1 **(H)**, Crk **(I)**, Ckap2 **(J)**, Parp14 **(K)**, and Mfn1 **(L)**, on cluster 1 of tumors from mice treated with PBS or S-V9 mAb

humans exhibited elevated levels of circulating FABP4, suggesting that tumors mobilized adipose tissue lipolysis for their growth benefits [16]. These studies indicate that targeting circulating FABP4 with monoclonal antibodies offers a promising strategy for blocking FABP4-mediated effects in both lean and obese subjects.

Although anti-FABP4 antibodies developed in rabbits showed treatment efficacy in animal studies, these

non-human antibodies cannot be used in clinical trials or for clinical treatment due to their immunogenicity in humans. To reduce immunogenicity without losing the antibody/antigen-specific binding property, we developed the first humanized anti-FABP4 antibodies in current studies. As an evolutionarily conservative protein, FABP4 shares high homology between animals and humans [19]. To expand the antibody repertoire targeting effective epitopes of FABP4, FABP4 knockout mice were used for human FABP4 immunization in current studies. After screening over 1200 hybridoma clones, we identified multiple anti-FABP4 monoclonal antibodies. Upon sequencing these antibodies, mouse/human chimeric antibodies consisting of mouse variable domains with human IgG1 constant region domain were developed. Of note, 12G2 clone exhibited a significant therapeutic efficacy by inhibiting tumor growth in a range of syngeneic and xenograft mouse models. To further improve the therapeutic and clinical potential, we generated 16 humanized 12G2 antibody variants by grafting its CDRs into the closest-matching human framework sequences. To assess their blocking function using in vitro cellular studies, we identified that the 12G2-V9 variant exhibited significant inhibition of FABP4-mediated tumor migration and proliferation in wound healing assays. Using various mouse models, we confirmed that V9 antibody had the most therapeutic efficacy by inhibiting mammary tumor growth. Given that most cancer death is due to metastasis [40], we further demonstrated that V9 treatment significantly inhibited tumor lung metastasis. Using spatial transcriptome analysis, we showed that V9 treatment induced abnormal mitochondrial respiration in tumor cells, contributing to tumor cell death. Epitope analysis of V9 binding to FABP4 indicated that V9 uniquely bound to β1, β-3/4, and β-7, potentially affecting fatty acid transport, lipid metabolism and signaling in tumor cells.

During our studies, there were several observations that are worth noting: (1) there were multiple anti-FABP4 mAbs which showed higher binding affinity to FABP4 than 12G2, but high affinity did not always translate into high efficacy in tumor treatment. Antigen-binding epitopes seem to be more relevant to the FABP4 blocking activity in vivo. (2) 12G2 inhibited tumor growth in multiple mouse models, including E0771, MMT, MCF-7, but did not appear to be effective for treatment of 4T1 model. It is likely that blocking lipid metabolism by 12G2 does not affect tumor cells, such as 4T1 cells, which exhibit greater metabolic plasticity and can adapt to using glucose and glutamine for rapid cell proliferation [41]. (3) Using the doses ranging from 5 to 30 mg/kg in different mouse models, we did not notice any obvious side effects, such as mouse death, reduced body weight, cytokine storm or local skin reactions. We are therefore optimistic that severe adverse effects in future clinical applications will be minimal. Moreover, given the pathogenic role of FABP4 in obesity-associated diseases, including diabetes, atherosclerosis and other cardiovascular diseases. [42, 43], the humanized anti-FABP4 antibodies we generated in this study are expected to have broader applications beyond breast cancer treatment.

Conclusions

In summary, we identified FABP4 as a new adipokine promoting breast cancer development and developed the first humanized anti-FABP4 monoclonal antibodies for treating breast cancer in mouse models. Blocking circulating FABP4 with monoclonal antibodies might represent a novel therapeutic strategy for treatment of breast cancer.

Abbreviations

FABP4	Fatty acid binding protein 4
aP2	Adipocyte protein 2
IGFs	Insulin/insulin-like growth factors
CDRs	Complementary determining regions
mAb	Monoclonal antibody
S-V9	Stable cell pool of V9 antibody
CHO	Chinese hamster ovary cells
K_D	Dissociation constant
HR	Hormone receptors
HER2	Human epidermal growth factor receptor 2

Supplementary Information

The online version contains supplementary material available at https://doi.org/10.1186/s13058-024-01873-y.

Supplementary Material 1

Supplementary Material 2

Acknowledgements

The authors would like to thank Iowa Institute of Human Genetics: Genomics Division and Iowa NeuroImaging Processing Core for providing 10x Genomics Visium Spatial Transcriptomics Service.

Author contributions

These authors contribute equally to the paper: J.H., R.J., Y.Y. Conceptualization: B.L. Methodology: J.H., R.J., Y.Y., X.J., Z.X, and N.S. Spatial RNA sequence analysis: M.C. Writing—original draft: B.L. Writing—review and editing: S.S. Supervision: B.L. Funding acquisition: B.L., S.S. All authors read and approved the final manuscript.

Funding

National Institutes of Health grant R01AI137324 (BL), R01CA180986 (BL) and U01CA272424 (BL).

Data availability

The four visium libraries (two PBS tumors, and two S-V9-treated tumors) were sequenced on an Illumina NovaSeq 6000 located in the Iowa Institute of Human Genetics (IIHG) Genomics division. Paired-end reads were demultiplexed and converted from the native Illumina BCL format to fastq format using an in-house python wrapper to Illumina's 'bcl2fastq' conversion utility. The data were deposited to GEO repository (GSE264099).

Declarations

Ethics approval and consent to participate

All experiments were performed according to the approval by the institutional review board at the University of Iowa, Iowa City, IA. Mouse experiments were performed according to protocols approved by the Institutional Animal Care and Use Committee at the University of Iowa, Iowa City, IA.

Consent for publication

Not applicable.

Competing interests

The authors declare no competing interests.

Author details

[1]Department of Pathology, University of Iowa, 431 Newton Road, Iowa City, IA 52242, USA
[2]Department of Immunology, School of Basic Medical Sciences, Peking University, Beijing, China
[3]School of Basic Medical Sciences, Guangdong Medical University, Zhanjiang, China
[4]Protein and Crystallography Facility, University of Iowa, Iowa City, IA, USA
[5]Iowa Institute of Human Genetics, University of Iowa, Iowa City, IA, USA
[6]Department of Surgery, University of Iowa, Iowa City, IA, USA

Received: 9 May 2024 / Accepted: 18 July 2024
Published online: 25 July 2024

References

1. Arnold M, Morgan E, Rumgay H, Mafra A, Singh D, Laversanne M, Vignat J, Gralow JR, Cardoso F, Siesling S, Soerjomataram I. Current and future burden of breast cancer: global statistics for 2020 and 2040. Breast. 2022;66:15–23. PubMed PMID: 36084384; PMCID: PMC9465273.
2. Lima SM, Kehm RD, Terry MB. Global breast cancer incidence and mortality trends by region, age-groups, and fertility patterns. EClinicalMedicine. 2021;38:100985. https://doi.org/10.1016/j.eclinm.2021.100985. Epub 20210707.
3. Loos RJF, Yeo GSH. The genetics of obesity: from discovery to biology. Nat Rev Genet. 2022;23(2):120–33. https://doi.org/10.1038/s41576-021-00414-z. Epub 20210923.
4. Albuquerque D, Nobrega C, Manco L, Padez C. The contribution of genetics and environment to obesity. Br Med Bull. 2017;123(1):159–73. https://doi.org/10.1093/bmb/ldx022. PubMed PMID: 28910990.
5. Buckley J. Availability of high-fat foods might drive the obesity epidemic. Nat Rev Endocrinol. 2018;14(10):574-5. https://doi.org/10.1038/s41574-018-0084-3. PubMed PMID: 30158548.
6. Hu S, Wang L, Yang D, Li L, Togo J, Wu Y, Liu Q, Li B, Li M, Wang G, Zhang X, Niu C, Li J, Xu Y, Couper E, Whittington-Davies A, Mazidi M, Luo L, Wang S, Douglas A, Speakman JR. Dietary Fat, but Not Protein or Carbohydrate, Regulates Energy Intake and Causes Adiposity in Mice. Cell Metab. 2018;28(3):415–. https://doi.org/10.1016/j.cmet.2018.06.010. Epub 2018/07/19. 31 e4.
7. Lee MJ, Wu Y, Fried SK. Adipose tissue remodeling in pathophysiology of obesity. Curr Opin Clin Nutr Metab Care. 2010;13(4):371–6. https://doi.org/10.1097/MCO.0b013e32833aabef. PubMed PMID: 20531178; PMCID: PMC3235038. Epub 2010/06/10.
8. Khandekar MJ, Cohen P, Spiegelman BM. Molecular mechanisms of cancer development in obesity. Nat Rev Cancer. 2011;11(12):886–95. https://doi.org/10.1038/nrc3174. Epub 2011/11/25.
9. Picon-Ruiz M, Morata-Tarifa C, Valle-Goffin JJ, Friedman ER, Slingerland JM. Obesity and adverse breast cancer risk and outcome: mechanistic insights and strategies for intervention. CA Cancer J Clin. 2017;67(5):378–97. PubMed PMID: 28763097; PMCID: PMC5591063.
10. Bianchini F, Kaaks R, Vainio H. Overweight, obesity, and cancer risk. Lancet Oncol. 2002;3(9):565–74. Epub 2002/09/10. doi: https://doi.org/10.1016/s1470-2045(02)00849-5. PubMed PMID: 12217794.
11. Calle EE, Kaaks R. Overweight, obesity and cancer: epidemiological evidence and proposed mechanisms. Nat Rev Cancer. 2004;4(8):579–91. https://doi.org/10.1038/nrc1408. Epub 2004/08/03.
12. Louie SM, Roberts LS, Nomura DK. Mechanisms linking obesity and cancer. Biochim Biophys Acta. 2013;1831(10):1499–508. https://doi.org/10.1016/j.bbalip.2013.02.008. Epub 20130305.
13. Park J, Morley TS, Kim M, Clegg DJ, Scherer PE. Obesity and cancer–mechanisms underlying tumour progression and recurrence. Nat Rev Endocrinol. 2014;10(8):455–65. https://doi.org/10.1038/nrendo.2014.94. Epub 20140617.
14. Roberts DL, Dive C, Renehan AG. Biological mechanisms linking obesity and cancer risk: new perspectives. Annu Rev Med. 2010;61:301–16. https://doi.org/10.1146/annurev.med.080708.082713. PubMed PMID: 19824817.
15. Zeng J, Sauter ER, Li B. FABP4: a new player in obesity-Associated breast Cancer. Trends Mol Med. 2020;26(5):437–40. https://doi.org/10.1016/j.molmed.2020.03.004. Epub 2020/05/04.
16. Hao J, Zhang Y, Yan X, Yan F, Sun Y, Zeng J, Waigel S, Yin Y, Fraig MM, Egilmez NK, Suttles J, Kong M, Liu S, Cleary MP, Sauter E, Li B. Circulating adipose fatty acid binding protein is a New Link underlying obesity-Associated Breast/Mammary Tumor Development. Cell Metab. 2018;28(5):689–705. https://doi.org/10.1016/j.cmet.2018.07.006. e5. Epub 2018/08/14.
17. Hao J, Yan F, Zhang Y, Triplett A, Zhang Y, Schultz DA, Sun Y, Zeng J, Silverstein KAT, Zheng Q, Bernlohr DA, Cleary MP, Egilmez NK, Sauter E, Liu S, Suttles J, Li B. Expression of Adipocyte/Macrophage fatty acid-binding protein in Tumor-Associated macrophages promotes breast Cancer Progression. Cancer Res. 2018;78(9):2343–55. https://doi.org/10.1158/0008-5472.CAN-17-2465. Epub 2018/02/14.
18. Hotamisligil GS, Bernlohr DA. Metabolic functions of FABPs–mechanisms and therapeutic implications. Nat Rev Endocrinol. 2015;11(10):592–605. https://doi.org/10.1038/nrendo.2015.122. Epub 2015/08/12.
19. Li B, Hao J, Zeng J, Sauter ER, SnapShot:. FABP Funct Cell. 2020;182(4):1066. https://doi.org/10.1016/j.cell.2020.07.027. PubMed PMID: 32822569; PMCID: PMC7439965. - e1Epub 2020/08/22.
20. Hao J. Thermal Shift Assay for Exploring Interactions Between Fatty Acid-Binding Protein and Inhibitors. Methods Mol Biol. 2021;2261:395–409. https://doi.org/10.1007/978-1-0716-1186-9_24. PubMed PMID: 33421003.
21. Loveless BC, Mason JW, Sakurai T, Inoue N, Razavi M, Pearson TW, Boulanger MJ. Structural characterization and epitope mapping of the glutamic acid/alanine-rich protein from Trypanosoma congolense: defining assembly on the parasite cell surface. J Biol Chem. 2011;286(23):20658–65. https://doi.org/10.1074/jbc.M111.218941. Epub 20110406.
22. Perosa F, Carbone R, Ferrone S, Dammacco F. Purification of human immunoglobulins by sequential precipitation with caprylic acid and ammonium sulphate. J Immunol Methods. 1990;128(1):9–16. https://doi.org/10.1016/0022-1759(90)90458-8. PubMed PMID: 2324507.
23. McKinney MM, Parkinson A. A simple, non-chromatographic procedure to purify immunoglobulins from serum and ascites fluid. J Immunol Methods. 1987;96(2):271–8. https://doi.org/10.1016/0022-1759(87)90324-3. PubMed PMID: 3805742.
24. Forouzanfar MH, Foreman KJ, Delossantos AM, Lozano R, Lopez AD, Murray CJ, Naghavi M. Breast and cervical cancer in 187 countries between 1980 and 2010: a systematic analysis. Lancet. 2011;378(9801):1461–84. https://doi.org/10.1016/S0140-6736(11)61351-2. Epub 20110914.
25. Jin R, Hao J, Yi Y, Yin D, Hua Y, Li X, Bao H, Han X, Egilmez NK, Sauter ER, Li B. Dietary Fats High in Linoleic acids impair antitumor T-cell responses by inducing E-FABP-Mediated mitochondrial dysfunction. Cancer Res. 2021;81(20):5296–310. https://doi.org/10.1158/0008-5472.CAN-21-0757. Epub 20210816.
26. Liu L, Jin R, Hao J, Zeng J, Yin D, Yi Y, Zhu M, Mandal A, Hua Y, Ng CK, Egilmez NK, Sauter ER, Li B. Consumption of the Fish Oil High-Fat Diet Uncouples Obesity and mammary tumor growth through induction of reactive oxygen species in Protumor Macrophages. Cancer Res. 2020;80(12):2564–74. https://doi.org/10.1158/0008-5472.CAN-19-3184. Epub 2020/03/28.
27. Hu Y, Smyth GK. ELDA: extreme limiting dilution analysis for comparing depleted and enriched populations in stem cell and other assays. J Immunol Methods. 2009;347(1–2):70 – 8. Epub 20090628. https://doi.org/10.1016/j.jim.2009.06.008. PubMed PMID: 19567251.
28. Tong CWS, Wu M, Cho WCS, To KKW. Recent advances in the treatment of breast Cancer. Front Oncol. 2018;8:227. Epub 20180614. doi: 10.3389/fonc.2018.00227. PubMed PMID: 29963498; PMCID: PMC6010518.
29. Yersal O, Barutca S. Biological subtypes of breast cancer: prognostic and therapeutic implications. World J Clin Oncol. 2014;5(3):412–24. https://doi.org/10.5306/wjco.v5.i3.412. PubMed PMID: 25114856; PMCID: PMC4127612.
30. Waks AG, Winer EP. Breast Cancer Treatment: A Review. JAMA. 2019;321(3):288–300. https://doi.org/10.1001/jama.2018.19323. PubMed PMID: 30667505.

31. Pascual G, Avgustinova A, Mejetta S, Martin M, Castellanos A, Attolini CS, Berenguer A, Prats N, Toll A, Hueto JA, Bescos C, Di Croce L, Benitah SA. Targeting metastasis-initiating cells through the fatty acid receptor CD36. Nature. 2017;541(7635):41–5. https://doi.org/10.1038/nature20791. Epub 20161207.
32. Luo X, Cheng C, Tan Z, Li N, Tang M, Yang L, Cao Y. Emerging roles of lipid metabolism in cancer metastasis. Mol Cancer. 2017;16(1):76. https://doi.org/10.1186/s12943-017-0646-3. Epub 20170411.
33. Sulsky R, Magnin DR, Huang Y, Simpkins L, Taunk P, Patel M, Zhu Y, Stouch TR, Bassolino-Klimas D, Parker R, Harrity T, Stoffel R, Taylor DS, Lavoie TB, Kish K, Jacobson BL, Sheriff S, Adam LP, Ewing WR, Robl JA. Potent and selective biphenyl azole inhibitors of adipocyte fatty acid binding protein (aFABP). Bioorg Med Chem Lett. 2007;17(12):3511–5. https://doi.org/10.1016/j.bmcl.2006.12.044. Epub 20061221.
34. Furuhashi M, Tuncman G, Gorgun CZ, Makowski L, Atsumi G, Vaillancourt E, Kono K, Babaev VR, Fazio S, Linton MF, Sulsky R, Robl JA, Parker RA, Hotamisligil GS. Treatment of diabetes and atherosclerosis by inhibiting fatty-acid-binding protein aP2. Nature. 2007;447(7147):959–65. https://doi.org/10.1038/nature05844. Epub 2007/06/08.
35. Okamura Y, Otani K, Sekiguchi A, Kogane T, Kakuda C, Sakamoto Y, Kodama T, Okada M, Yamawaki H. Vasculo-protective effect of BMS-309403 is independent of its specific inhibition of fatty acid-binding protein 4. Pflugers Arch. 2017;469(9):1177–88. https://doi.org/10.1007/s00424-017-1976-0. Epub 20170413.
36. Lin W, Huang X, Zhang L, Chen D, Wang D, Peng Q, Xu L, Li J, Liu X, Li K, Ding K, Jin S, Li J, Wu D. BMS309403 stimulates glucose uptake in myotubes through activation of AMP-activated protein kinase. PLoS ONE. 2012;7(8):e44570. https://doi.org/10.1371/journal.pone.0044570. Epub 20120831.
37. Look C, Morano I, Ehrhart-Bornstein M, Bornstein SR, Lamounier-Zepter V. BMS309403 directly suppresses cardiac contractile function. Naunyn Schmiedebergs Arch Pharmacol. 2011;384(3):255–63. https://doi.org/10.1007/s00210-011-0667-1. Epub 20110716.
38. Cao H, Sekiya M, Ertunc ME, Burak MF, Mayers JR, White A, Inouye K, Rickey LM, Ercal BC, Furuhashi M, Tuncman G, Hotamisligil GS. Adipocyte lipid chaperone AP2 is a secreted adipokine regulating hepatic glucose production. Cell Metab. 2013;17(5):768–78. PubMed PMID: 23663740; PMCID: PMC3755450.
39. Burak MF, Inouye KE, White A, Lee A, Tuncman G, Calay ES, Sekiya M, Tirosh A, Eguchi K, Birrane G, Lightwood D, Howells L, Odede G, Hailu H, West S, Garlish R, Neale H, Doyle C, Moore A, Hotamisligil GS. Development of a therapeutic monoclonal antibody that targets secreted fatty acid-binding protein aP2 to treat type 2 diabetes. Sci Transl Med. 2015;7(319):319ra205. https://doi.org/10.1126/scitranslmed.aac6336. Epub 2015/12/25.
40. Dillekas H, Rogers MS, Straume O. Are 90% of deaths from cancer caused by metastases? Cancer Med. 2019;8(12):5574–6. Epub 20190808. doi: https://doi.org/10.1002/cam4.2474. PubMed PMID: 31397113; PMCID: PMC6745820.
41. Simoes RV, Serganova IS, Kruchevsky N, Leftin A, Shestov AA, Thaler HT, Sukenick G, Locasale JW, Blasberg RG, Koutcher JA, Ackerstaff E. Metabolic plasticity of metastatic breast cancer cells: adaptation to changes in the microenvironment. Neoplasia. 2015;17(8):671–84. PubMed PMID: 26408259; PMCID: PMC4674487.
42. Powell-Wiley TM, Poirier P, Burke LE, Despres JP, Gordon-Larsen P, Lavie CJ, Lear SA, Ndumele CE, Neeland IJ, Sanders P, St-Onge MP, American Heart Association Council on L, Cardiometabolic H, Council C, Stroke N. Council on Clinical C, Council on E, Prevention, Stroke C. Obesity and Cardiovascular Disease: A Scientific Statement From the American Heart Association. Circulation. 2021;143(21):e984-e1010. Epub 20210422. doi: https://doi.org/10.1161/CIR.0000000000000973. PubMed PMID: 33882682; PMCID: PMC8493650.
43. Silveira EA, Kliemann N, Noll M, Sarrafzadegan N, de Oliveira C. Visceral obesity and incident cancer and cardiovascular disease: an integrative review of the epidemiological evidence. Obes Rev. 2021;22(1):e13088. https://doi.org/10.1111/obr.13088. Epub 20200721.

Publisher's Note